Supplementary Information

Rational Design of Main Chain Conjugated Copolymer Having Donor-Acceptor Heterojunctions and its Application to Indoor Photovoltaic Cells

Na Yeon Kwon [a], Su Hong Park [a], Hungu Kang [a], Ashkan Vakilipour Takaloo [b], Amit Kumar Harit [a], Han Young Woo [a], Tae Geun Kim [b], Hyo Jae Yoon [a], Min Ju Cho *[,a] and Dong Hoon Choi *[,a]

[a] *Department of Chemistry, Research Institute for Natural Sciences, Korea University, 145 Anam-Ro, Sungbuk-gu, Seoul 02841 South Korea*

[b] *School of Electrical Engineering, Korea University, 145 Anam-Ro, Sungbuk-gu, Seoul 02841 South Korea*

Corresponding Author

*Corresponding authors: M. J. Cho (chominju@korea.ac.kr), D. H. Choi (dhchoi8803@korea.ac.kr)

Experimental Section

Materials

All chemicals used for the synthesis of P(BDBT), P(NDI2T) and P(BDBT-*co*-NDI2T) were purchased from Sigma-Aldrich, Acros Organics Co., and Tokyo Chemical Industry and used without further purification. The reagent grade solvents used in this experiment were freshly dried using standard distillation methods.

Synthesis

Polymerization of P(NDI2T)

For the synthesis of P(NDI2T) for making blend films, M1 (205.10 mg, 20.82 mmol, 1 eq.) and M2 (102.41 mg, 20.82 mmol, 1 eq.) were dissolved in a mixture of dry toluene (5 mL) by adding $Pd(PPh_3)_4$. The reaction mixture was heated and stirred for 6 h at 110 °C. Then, the solution was cooled and precipitated in methanol (300 mL). The unreacted monomer and oligomers were separated using the Soxhlet extraction method with acetone, n-hexane, and methylene chloride (MC) sequentially. The extracted MC fraction was precipitated into methanol (300 mL) and dried in vacuo at 60 °C for 24 h (P(NDI2T): M_n of 46.1 kg mol^{-1}; PDI of 2.43).

Polymerization of P(BDBT)

For the synthesis of P(BDBT) for making blend films, M3 (188.34 mg, 20.82 mmol, 1 eq.), M4 (100.02 mg, 20.82 mmol, 1 eq.), and $Pd(PPh_3)_4$ were added to a Schlenk tube. Dry toluene

(5 mL) was then added and the mixture was degassed. The reactor was stirred and refluxed for 24 h at 110 °C. After cooling to RT, the resulting solution was precipitated into methanol (300 mL). The byproducts, namely, the unreacted monomer and oligomers, were removed through a Soxhlet extraction method using acetone, n-hexane, methylene chloride, and chloroform successively. The concentrated chloroform fraction was then precipitated into methanol (300 mL) and dried under a vacuum at 60 °C for 24 h (P(BDBT): M_n of 43.1 kg mol^{-1}; PDI of 4.51).

Polymerization of P(BDBT-*co*-NDI2T)

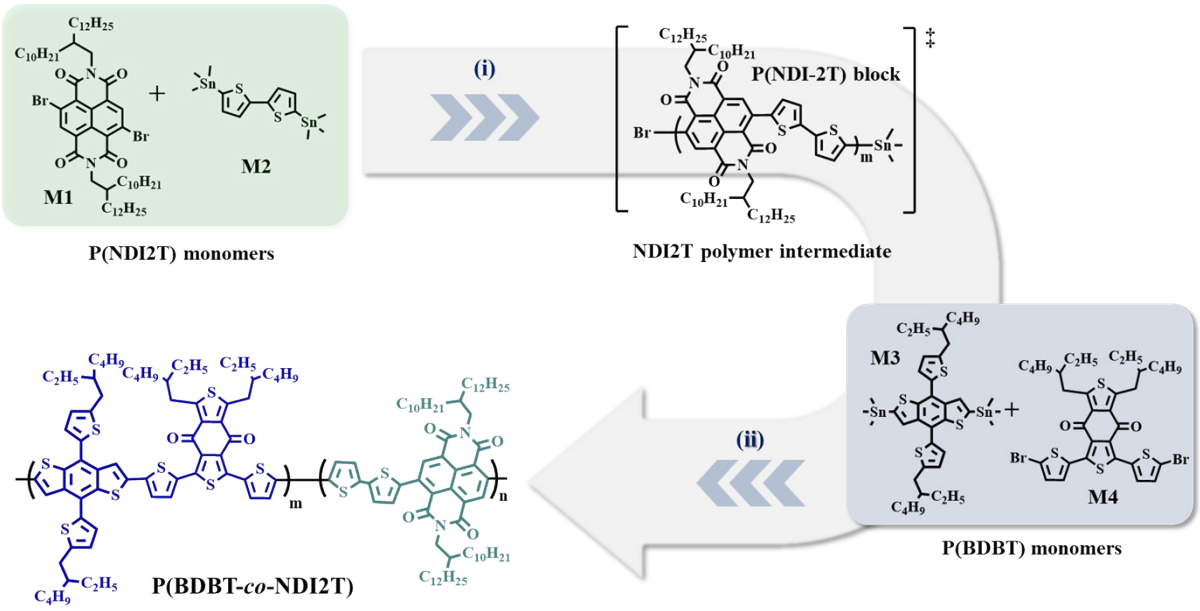

Scheme S1. (a) Synthesis procedure of P(BDBT-*co*-NDI2T). (i) Pd(pph$_3$)$_4$, toluene, 110 °C, 6 h. (ii) Injection of M3 and M4.

To prepare the NDI2T polymer intermediate, M1 (205.10 mg, 20.82 mmol, 1 eq.), M2 (102.41 mg, 20.82 mmol, 1 eq.), and Pd(PPh$_3$)$_4$ were dissolved in toluene (5 mL) and the reaction mixture was degassed. The temperature was gradually increased to 110 °C while

stirring the reaction mixture. After 6 h, the mixed toluene solution (3 mL) of M3 (188.34 mg, 20.82 mmol, 1 eq.) and M4 (100.02 mg, 20.82 mmol, 1 eq.) was added to a reactor. The reaction mixture was kept under stirring at 110 °C for 48 h. The resulting solution was cooled and precipitated in methanol (300 mL). The relatively low molecular weight polymers, byproducts and residual catalysts were eliminated through a Soxhlet extraction with acetone, hexane, methylene chloride, and chloroform. The chloroform fraction was then poured into methanol (300 mL) and the precipitated products were dried in vacuo at 60 °C for 24 h. (P(BDBT-*co*-NDI2T): M_n of 42.2 kg mol^{-1}; PDI of 3.59). Elemental Anal. Found for $(C_{68}H_{78}O_2S_8)_m$-$(C_{70}H_{104}N_2O_4S_2)_n$: C, 71.67; H, 7.69; N, 0.93; S, 15.85; m:n ≈ 2:1.

Characterization and measurements

Instrumentation

^{1}H NMR spectra were recorded using a Bruker 500 MHz spectrometer (Ascend 500, Bruker) for structural analyses of all synthesized compounds. The number average molecular weights (M_n) and PDIs of P(BDBT), P(NDI2T), and P(BDBT-*co*-NDI2T) were estimated using gel permeation chromatography (GPC; Agilent GPC 1200 series) at 80 °C with *o*-dichlorobenzene (*o*-DCB) as the eluent and polystyrene (PS) as the standard. The absorption spectra of P(BDBT), P(NDI2T), and P(BDBT-*co*-NDI2T) in chloroform (CF) and thin films were recorded using a UV−vis absorption spectrometer (Agilent 8453, photodiode array, λ = 190−1100 nm). Thermal properties, including the glass-transition temperature (T_g) and decomposition temperature (T_d), were measured by SCINCO TGA-N 1000 and Mettler DSC 821e instruments under N_2 conditions at a heating rate of 10 °C min^{-1}. The electrochemical

properties were characterized through cyclic voltammetry (CV, eDAQ EA161) using an electrolyte solution prepared by dissolving tetrabutylammonium hexafluorophosphate (Bu_4NPF_6) in acetonitrile. A Pt wire and Ag/AgCl were used as the counter and reference electrodes, respectively.

TEM was applied to observe the internal morphology of thin films (Tecnai G2F30 transmission electron microscope, FEI Inc.; accelerating voltage = 300 kV). The samples used for TEM observations were prepared by coating a carbon-coated copper grid with the polymer solution. KPFM measurements were carried out in ambient conditions, using a Bruker AFM Multimode model in amplitude-modulated KPFM. Pt/Ir coated conductive probes (SCM-PIT-V2, spring constant 3 N/m, resonant frequency 75 kHz, Bruker) were calibrated on freshly cleaved highly oriented pyrolytic graphite (HOPG) to determine the work function of the tip. Topography and KPFM data were obtained simultaneously using a standard two-pass procedure, where a topographic line was first acquired in tapping mode and a KPFM line was secondly acquired in a lift mode. In the lift mode, the tip scanned at a constant distance of 80 nm above the sample surface to ensure that electrostatic forces were dominant. In the KPFM mode, the applied AC voltage had an amplitude of 2000 mV at a frequency close to the resonance frequency of the cantilever (~70 kHz). In our KPFM configuration, negative changes of the contact potential difference (CPD) values indicated an increasing electron (negative charge) population at the sample surface, and vice versa. KPFM images of the sample surface were acquired at a probe scan rate of 0.5 Hz with scan size of 5 μm and 512 samples per line over five different regions. Grazing incidence wide-angle X-ray diffraction (GIWAXD) measurements were conducted at the 9 Å beamline (energy = 11.015 keV, pixel size = 88.6 μm, λ = 1.12199 Å, 2θ = 0−20°) of the Pohang Accelerator Laboratory. Films were prepared

by spin-coating the polymer solutions onto a SiO_2 wafer. The surface morphologies of the films were explored using an atomic force microscope (XE-100, Advanced Scanning Probe Microscope, PSIA) with a silicon cantilever.

PV device fabrication and characterization

The device was fabricated using a solution process and had an inverted device configuration of glass/ITO/ZnO/active layer/MoO_3/Ag. An ITO (150 nm)-coated glass was cleaned by ultrasonication sequentially in deionized water and isopropyl alcohol for 10 min. The dried ITO glass was subjected to UV−ozone treatment for 20 min. ZnO (40 nm) as an electron transport layer was spin-coated on the top of ITO glass using a ZnO precursor solution at 3,000 rpm for 40 s. After drying at 165 °C for 1 h, it was transferred to a glove box filled with nitrogen gas for use.

The active layer of the PSC was spin-coated on the ZnO layer in a 15 mg mL^{-1} anhydrous toluene solution. The prepared solution was then spin-coated onto the ZnO layer. The resulting active layer was 80−100 nm thick. Finally, a MoO_3 (10 nm) layer and Ag (100 nm) layer were deposited on the active layer using a thermal evaporator to form a 4 mm^2 active region through a shadow mask. The *J*−*V* curves of the devices were measured using a Keithley 2400 source meter under simulated AM 1.5G illumination (100 mW cm^{-2}) with the Oriel® Sol2A™ Class ABA solar simulator (Newport Corp.). The SimuLight® Solar simulator LED100 (McScience Inc.) was used to provide the LED light illumination. The lux levels of the LED lamps were measured using a TES-1330A luxmeter (TES Electronic Corp.). The external quantum efficiency (EQE) spectra were recorded using a certified EQE instrument (McScience Inc., EQX 3100).

Exciton Dissociation and Charge Carrier Recombination Behavior

The photocurrent density (J_{ph}) can be defined as $J_{ph} = J_L - J_D$, where J_L and J_D are the current densities under light illumination and in the dark, respectively. The effective voltage (V_{eff}) can be defined as $V_{eff} = V_0 - V_{bias}$, where V_0 is the voltage at which J_{ph} is zero and V_{bias} is the applied external voltage bias. When a high V_{eff} is applied to the device, the dissociated mobile charge carriers efficiently move toward the electrode with minimal recombination.[S1] The maximum exciton generation rates (G_{max}) can be estimated from the equation $J_{sat} = q \cdot L \cdot G_{max}$, where J_{sat} is the saturated photocurrent density, q is the electronic charge, and L is the thickness of the active layer in the devices.[S2]

Measurement of charge mobility through space-charge-limited current (SCLC)

Hole-only devices with a structure of ITO/PEDOT:PSS/active layer/Au and electron-only devices with a configuration of ITO/ZnO/active layer/LiF/Al were fabricated. The hole and electron carrier mobilities were determined using the modified Mott-Gurney equation, $J = (9/8)\varepsilon_0\varepsilon_r\mu(V^2/L^3)$, where J is the current density, μ is the mobility, and V is the applied voltage, and the device thickness, L, is defined. Moreover, ε_0 is the vacuum permittivity and ε_r is the relative permittivity. The mobility was calculated from the slope of the J–V plots. Using the modified Mott-Gurney equations, we determined the hole and electron carrier mobility by fitting the J–V curve in the near quadratic region.[S3]

Table S1. Number average molecular weight (M_n) and polydispersity index (PDI) data obtained from gel permeation chromatography.

Polymer	M_n [kg mol^{-1}]	PDI
NDI2T polymer intermediate [a]	39.8	2.34
P(BDBT-*co*-NDI2T)	42.2	3.59

[a] In the process of polymerization of P(BDBT-*co*-NDI2T), a small amount of NDI2T polymer intermediate was collected after polymerization of M1 and M2 for 6 hours and before adding M3 and M4 to the reactor.

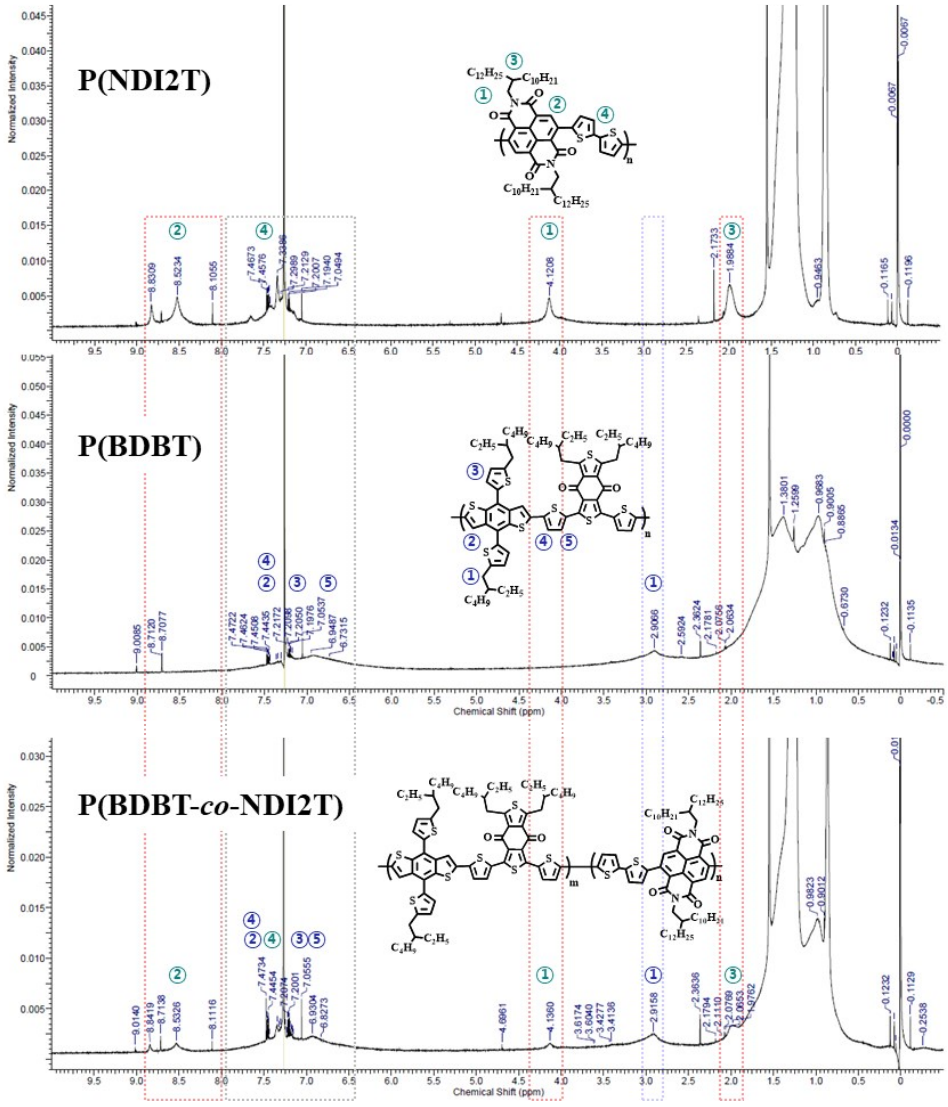

Figure S1 ^{1}H NMR spectra of P(NDI2T), P(BDBT), and P(BDBT-*co*-NDI2T).

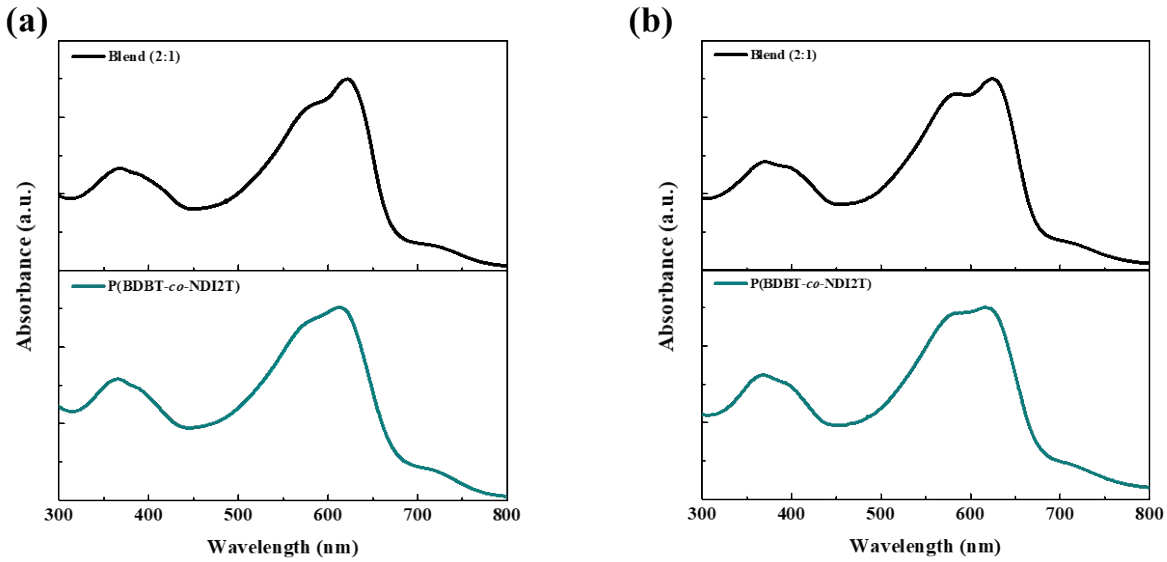

Figure S2. (a) UV-vis absorption spectra of the P(BDBT):P(NDI2T) (2:1) blend solution and copolymer in (a) chloroform solutions and (b) films.

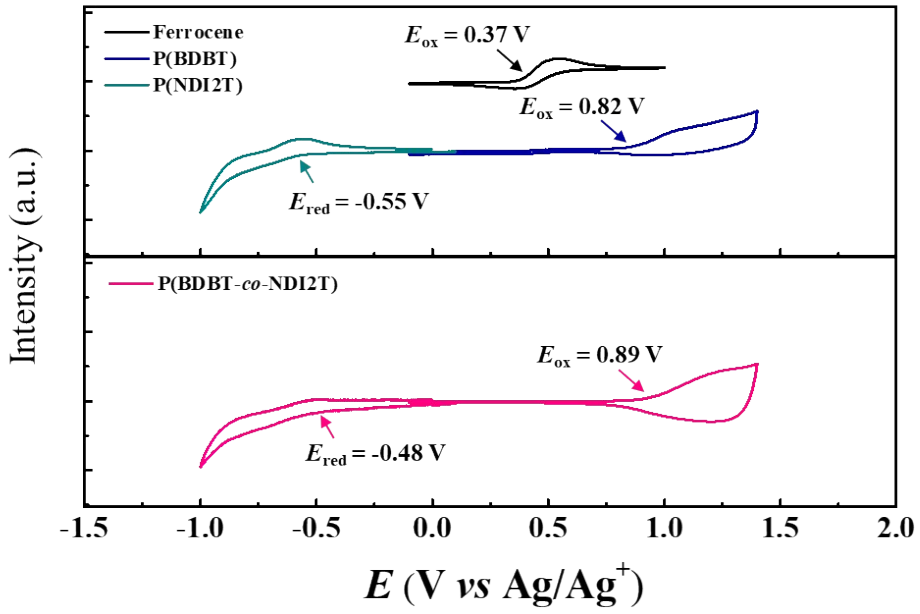

Figure S3. Cyclic voltammograms of P(BDBT), P(NDI2T) and P(BDBT-*co*-NDI2T).

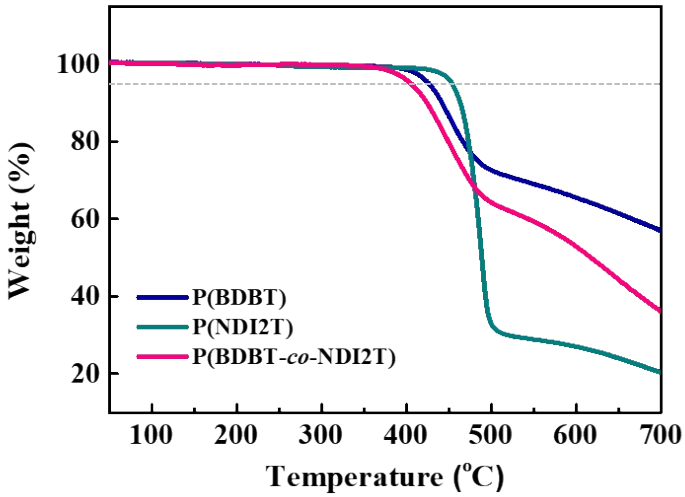

Figure S4. TGA curves of P(BDBT), P(NDI2T), and P(BDBT-*co*-NDI2T) with a heating rate of 10 °C min^{-1} under an inert atmosphere.

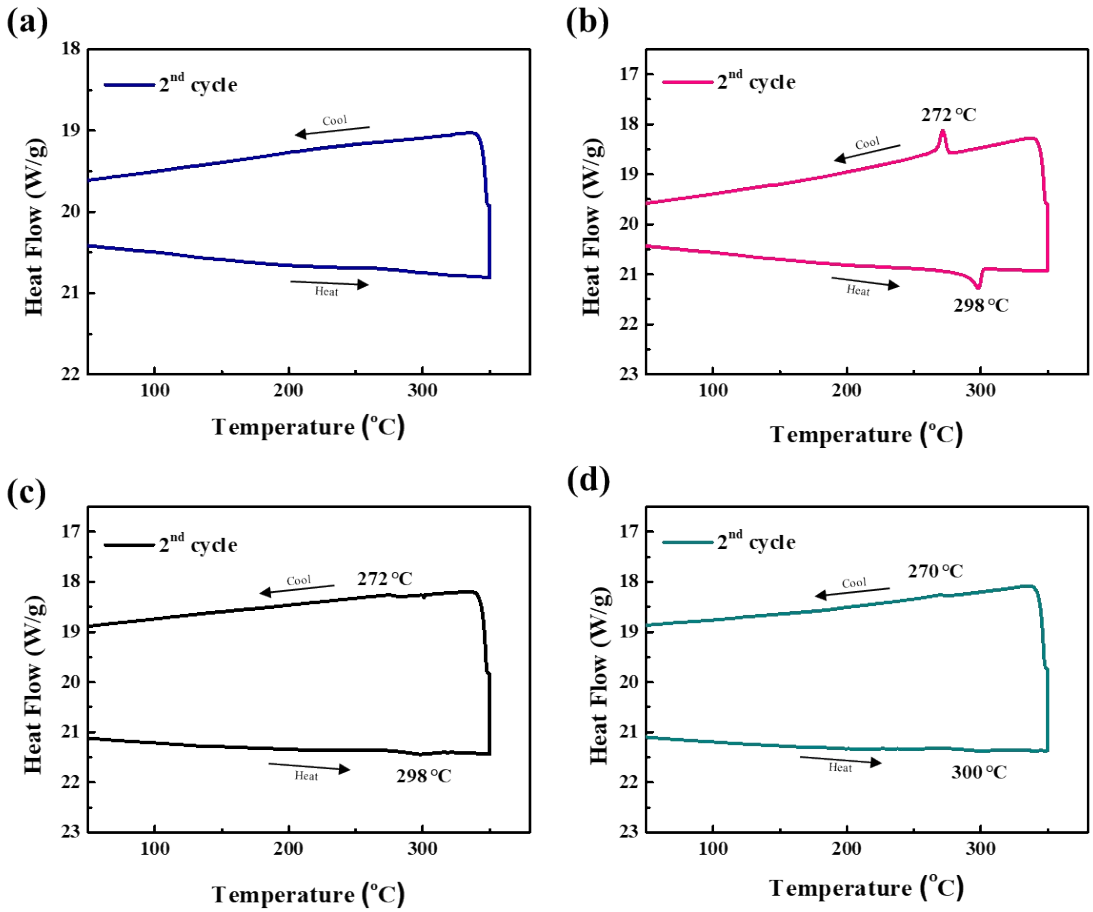

Figure S5. DSC thermograms of (a) P(BDBT), (b) P(NDI2T), (c) P(BDBT):P(NDI2T) blend (2:1), and (d) P(BDBT-*co*-NDI2T) measured with a scan rate of 10 °C min^{-1}.

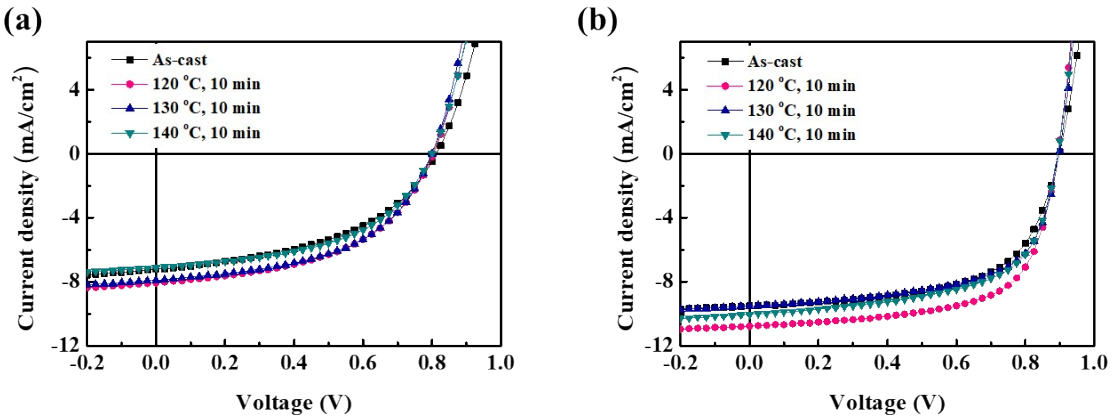

Figure S6. *J-V* characteristics of the PSCs with a photoactive layer of (a) P(BDBT):P(NDI2T) blend (2:1) and (b) P(BDBT-*co*-NDI2T) under AM 1.5G illumination at different annealing temperatures.

Table S2. Photovoltaic performance of the PSCs with a device structure of ITO/ZnO/Active layer/MoO_3/Ag under AM 1.5G illumination (100 mW cm^{-2}). The device active area was defined by a mask with an area of 4.00 mm^2.

Active layer	Treatment	V_{oc} [V]	J_{sc} [mA cm^{-2}]	FF	PCE [%]
P(BDBT) : P(NDI2T)	As-cast	0.81	7.21	0.47	2.74
	120 °C, 10 min	0.83	8.66	0.57	4.09
	130 °C, 10 min	0.79	7.91	0.51	3.18
	140 °C, 10 min	0.79	7.09	0.51	2.85
P(BDBT-*co*-NDI2T)	As-cast	0.88	10.62	0.58	5.42
	120 °C, 10 min	0.89	10.76	0.65	6.22
	130 °C, 10 min	0.89	9.52	0.62	5.25
	140 °C, 10 min	0.89	10.05	0.61	5.45

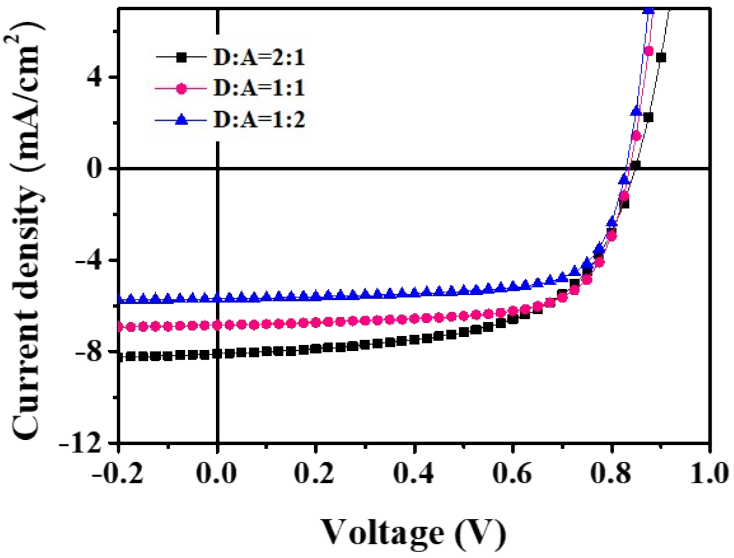

Figure S7. *J-V* characteristics of PSCs with a photoactive layer of P(BDBT):P(NDI2T) blend with different D/A weight ratios. *The active layer was annealed at 120 °C for 10 min.

Table S3. Photovoltaic performance of PSCs with a device structure of ITO/ZnO/Active layer/MoO_3/Ag under AM 1.5G illumination (100 mW cm^{-2}). Active layer: P(BDBT): P(NDI2T) with different D/A weight ratios. *The active layer was annealed at 120 °C for 10 min.

Active layer	D/A (w/w)	V_{oc} [V]	J_{sc} [mA cm^{-2}]	FF [%]	PCE [%]
P(BDBT) : P(NDI2T)	2:1	0.84	8.08	0.58	3.93
	1:1	0.83	6.84	0.69	3.91
	1:2	0.82	5.68	0.70	3.26

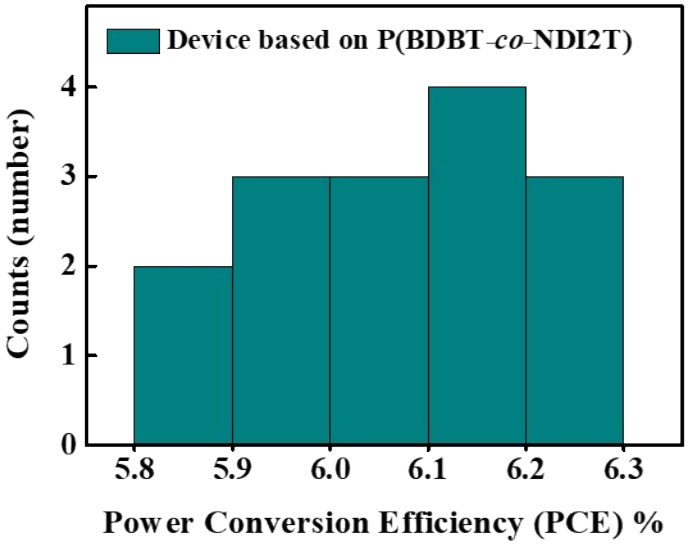

Figure S8. PCE distribution of optimized PSC devices under AM 1.5G illumination (100 mW cm^{-2}). The histogram shows the performance distribution of the 15 devices with the highest efficiency measured in this study. *The active layer was annealed at 120 °C for 10 min.

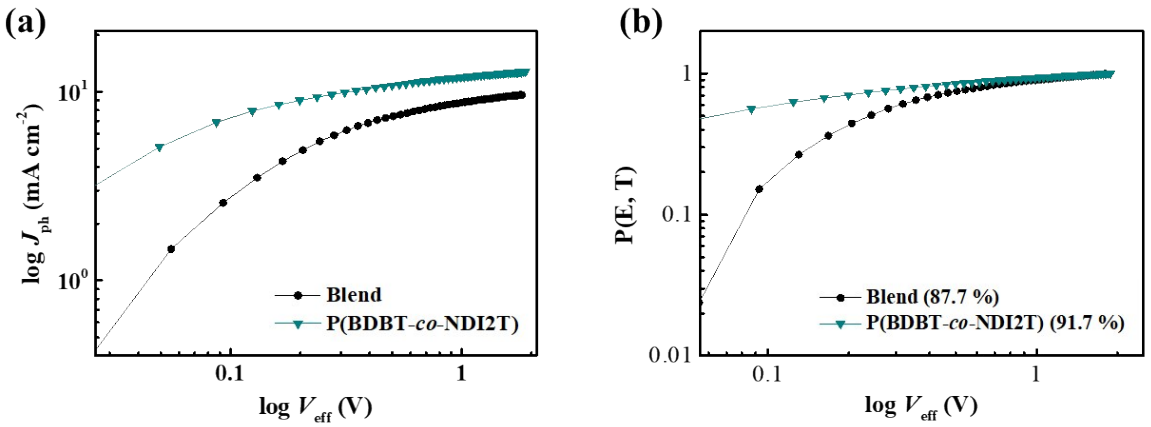

Figure S9. (a) Photocurrent density versus effective voltage characteristics of PSCs with a photoactive layer of P(BDBT):P(NDI2T) blend (2:1) and P(BDBT-*co*-NDI2T). (b)The exciton dissociation probability (Plots of J_{ph}/J_{sat} versus effective voltage (V_{eff})) of PSCs with a photoactive layer of P(BDBT):P(NDI2T) blend (2:1) and P(BDBT-*co*-NDI2T) under AM 1.5G illumination. *Thermal annealing at 120 °C for 10min

To better understand the superior performance of the P(BDBT-*co*-NDI2T)-based PSC device with a simple active layer, the exciton generation, exciton dissociation, and charge extraction properties were investigated through the dependence of the photocurrent density

(J_{ph}) on the sufficient voltage (V_{eff}) of the device (**Figure S8a)**. The annealed P(BDBT-*co*-NDI2T) and blend-based PSCs showed a saturation in the J_{ph} value, indicating that all photogenerated charge carriers are collected into the electrodes.

The exciton dissociation probability (P(E, T)) is concerned with the extent of charge carrier recombination in each device. Under the short-circuit condition, the annealed P(BDBT-*co*-NDI2T)-based device showed higher exciton dissociation probabilities ($P_{diss} = J_{ph}/J_{sat}$) of 91.7% relative to the annealed binary blend device (87.7%), which agrees well with the higher EQE (**Figure S8b**). This result indicates that the P(BDBT-*co*-NDI2T)-based PSC can efficiently decrease charge recombination, which partially contributes to the noticeably improved FF.

Table S4. Maximum exciton generation rate (G_{max}).

Active layer	J_{sat} [A m^{-2}]	q [A·s]	Thickness (L) [m]	G_{max} [m^{-3} s^{-1}]
P(BDBT):P(NDI2T)	96.83	1.602×10^{-19}	95×10^{-9}	6.36×10^{27}
P(BDBT-*co*-NDI2T)	127.94	1.602×10^{-19}	60×10^{-9}	1.33×10^{28}

This can lead us to obtain the maximum exciton generation rates (G_{max}) of the devices characterized herein. The calculated G_{max} values of the devices are summarized in **Table S4**. The P(BDBT-*co*-NDI2T)-based PSC showed the highest G_{max} value (1.33×10^{28} m^{-3} s^{-1}), which was much higher than the calculated G_{max} value for a blend-based PSC (6.36×10^{27} m^{-3} s^{-1}). The larger G_{max} value indicate that the exciton generation of the P(BDBT-*co*-NDI2T) film is faster than that of the P(BDBT):P(NDI2T) blend film device, which agrees with the corresponding higher J_{sc} values.

By analyzing the dependence of V_{oc} and J_{sc} on the light intensity (P_{light}), we observed a weak dependence of V_{oc} on P_{light} for the P(BDBT-*co*-NDI2T)-based device with a low slope of

1.01 kT/q, while that for the blend device is 2.16 kT/q (**Figure S9a**), where k, T, and q refer to the Boltzmann constant, Kelvin temperature, and unit charge, respectively.[S4] The smaller slope value of the P(BDBT-*co*-NDI2T)-based device (1.01 kT/q) indicates that trap-assisted recombination is suppressed more effectively.[S4-5]

The relationship between J_{sc} and incident light intensity (P_{light}= P_{in}) can be described as $J_{sc} \propto (P_{light})^{\alpha}$. When all charges are collected into the electrode before recombination, α should be equal to 1; thus, $\alpha < 1$ indicates that charge recombination occurs to a certain extent.[S6] The α value of the annealed P(BDBT-*co*-NDI2T) film based PSC is 0.98, indicating negligible bimolecular recombination and a more efficient charge carrier transportation feature in the simple active layer. In contrast, the annealed blend film-based device could be expected to exhibit a higher extent of bimolecular recombination with α value of 0.96. (**Figure S9b**)

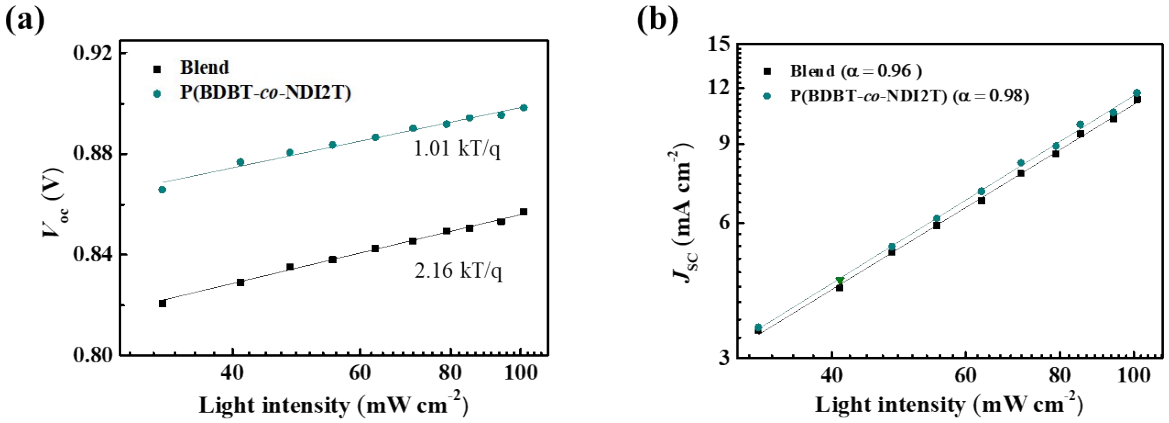

Figure S10. Light intensity dependent photovoltaic parameters: (a) V_{oc} and (b) J_{sc} for P(BDBT)**:**P(NDI2T) blend (2:1) and P(BDBT-*co*-NDI2T) under AM 1.5G illumination.

In **Table 2** and **Figure S10**, the values of two parasitic resistances: a series resistance (R_S) and a shunt resistance (R_{SH}) for the four different devices are summarized. The P(BDBT-*co*-NDI2T) film showed a decreasing tendency for R_S (9.23 Ω cm^2 to 6.97 Ω cm^2) and an

increasing tendency for R_{SH} (693.26 Ω cm^2 to 743.75 Ω cm^2) after the thermal annealing process. These data support the improvement of the FF values, which is approximately 0.65.[S7] The same tendency was observed in the blend films. Therefore, the current losses in the PSC made of an annealed film were reduced after the thermal annealing process, indicating that the current leakage from the boundary of the electrode was prevented and that better contacts exist between the active layer and the electrodes, with few defects.

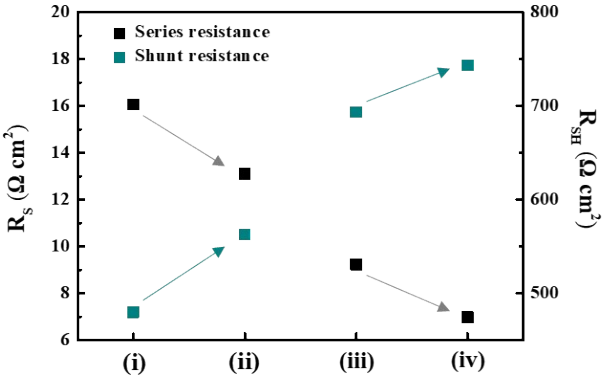

Active layer	R_S [Ω cm^2]	R_{SH} [Ω cm^2]
i	16.07	479.66
ii	13.10	562.58
iii	9.23	693.26
iv	6.97	743.75

Figure S11. R_S and R_{SH} of the device under AM 1.5G illumination. (i) As-cast blend film, (ii) annealed blend film, (iii) as-cast P(BDBT-*co*-NDI2T) film, (iv) annealed P(BDBT-*co*-NDI2T) film. *The active layer was annealed at 120 °C for 10 min.

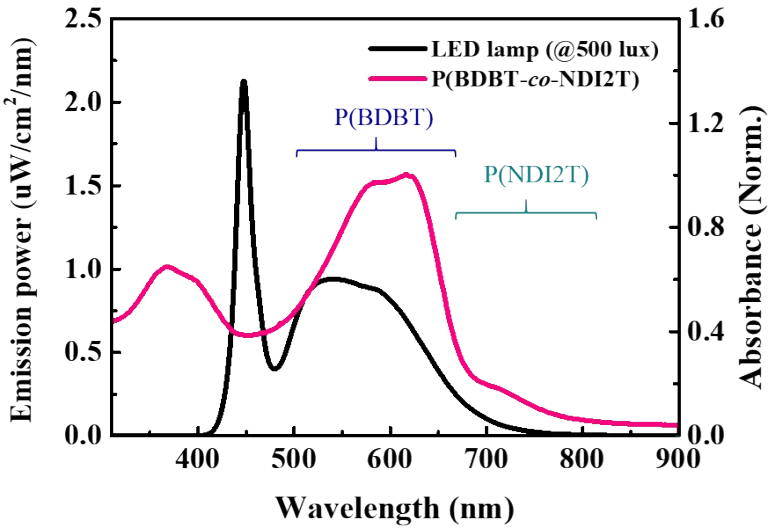

Figure S12. The radiative spectrum of the LED lamp (500 lux) used in this work, and the UV-*vis* absorption spectrum of P(BDBT-*co*-NDI2T) in the film state.

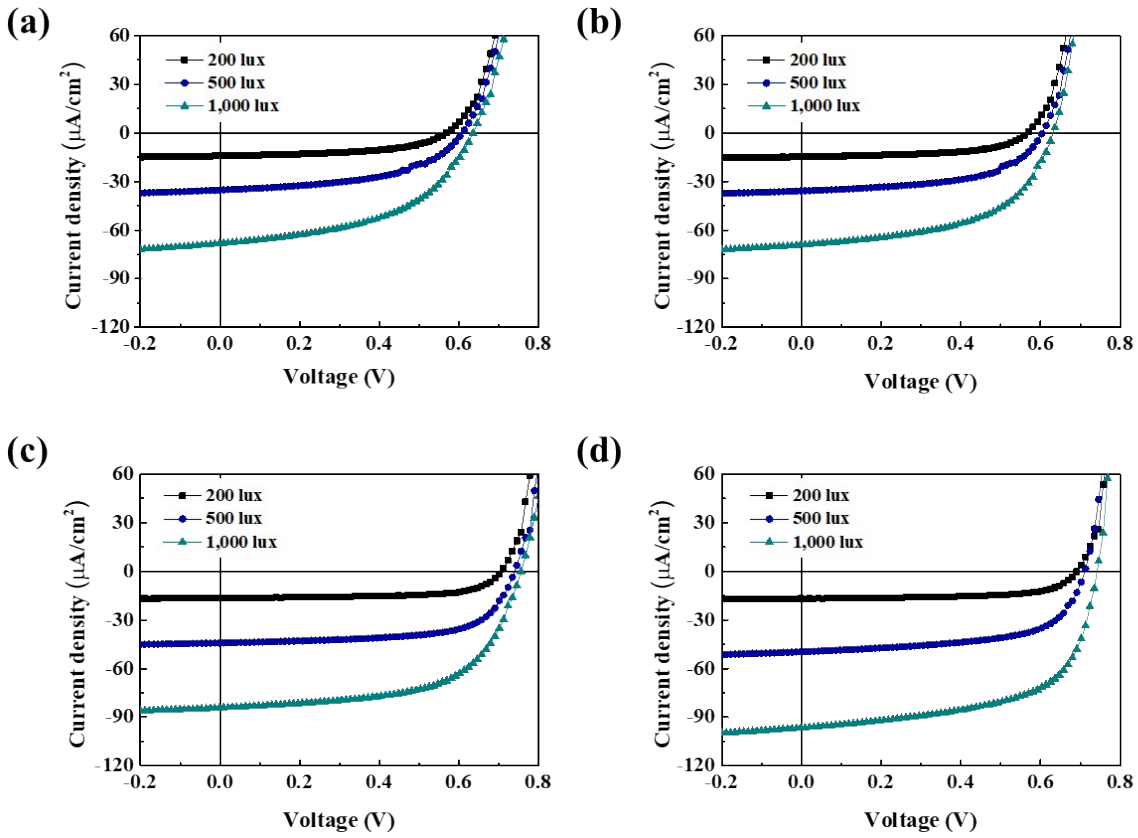

Figure S13. *J–V* characteristics of the IPVs with a photoactive layer of (a, b) P(BDBT)**:**P(NDI2T) blend (2:1) and (c, d) P(BDBT-*co*-NDI2T) under an LED lamp with 200 lux, 500 lux, and 1000 lux. *The active layer was annealed at 120 °C for 10 min.

Table S5. Photovoltaic performance of the IPVs with a device structure of ITO/ZnO/Active layer/MoO_3/Ag under LED lamps with different light intensities.

Active layer	Treatment	Intensity [lux]	P_{in} [μW cm^{-2}]	V_{oc} [V]	J_{sc} [μA cm^{-2}]	FF	P_{out} [a] [μW cm^{-2}]	PCE [b] [%]	R_S [Ω cm^2]	R_{SH} [Ω cm^2]
P(BDBT): P(NDI2T)	As-cast	200	68	0.55 (0.54 ± 0.02)	13.56 (11.84 ± 1.83)	0.48 (0.40 ± 0.04)	3.57	5.26 (4.21±1.25)	16.78	155.69
	120℃ 10 min			0.56 (0.55 ± 0.01)	14.49 (12.96 ± 1.21)	0.55 (0.53 ± 0.02)	4.46	6.56 (5.37±0.96)	12.10	174.63
P(BDBT-*co*-NDI2T)	As-cast			0.72 (0.71 ± 0.01)	16.30 (16.14 ± 0.65)	0.59 (0.56 ± 0.04)	6.92	10.18 (9.59±0.93)	13.45	309.44
	120℃ 10 min			0.69 (0.68 ± 0.01)	16.71 (15.96 ± 0.75)	0.66 (0.63 ± 0.03)	7.61	11.19 (10.41±0.60)	6.64	326.13
P(BDBT): P(NDI2T)	As-cast	500	170	0.63 (0.58 ± 0.01)	33.67 (32.64 ± 3.06)	0.46 (0.41 ± 0.05)	9.29	5.46 (4.79±1.06)	9.76	56.171
	120℃ 10 min			0.60 (0.59 ± 0.01)	36.08 (34.03 ± 2.42)	0.54 (0.50 ± 0.04)	11.68	6.87 (5.33±0.90)	4.58	70.89
P(BDBT-*co*-NDI2T)	As-cast			0.75 (0.75 ± 0.00)	45.40 (43.86 ± 0.80)	0.60 (0.57 ± 0.03)	20.43	12.02 (11.18±0.79)	5.75	110.11
	120℃ 10 min			0.71 (0.72 ± 0.01)	49.89 (47.42 ± 2.47)	0.61 (0.62 ± 0.01)	21.59	12.70 (12.12±0.37)	2.73	120.43
P(BDBT): P(NDI2T)	As-cast	1000	340	0.63 (0.61 ± 0.01)	66.60 (61.19 ± 5.50)	0.47 (0.39 ± 0.05)	19.72	5.80 (4.48±1.09)	6.23	30.67
	120℃ 10 min			0.63 (0.61 ± 0.02)	68.39 (64.56 ± 3.83)	0.53 (0.48 ± 0.05)	22.83	6.71 (5.70±0.93)	3.27	37.70
P(BDBT-*co*-NDI2T)	As-cast			0.76 (0.76 ± 0.00)	89.86 (83.58 ± 4.49)	0.59 (0.56 ± 0.03)	40.29	11.85 (10.60±1.05)	3.58	59.46
	120℃ 10 min			0.74 (0.74 ± 0.01)	96.55 (86.65 ± 7.46)	0.60 (0.60 ± 0.02)	42.86	12.61 (11.49±0.90)	1.71	62.43

[a] Maximum output power density, $P_{out} = J_{sc}$ x V_{oc} x FF. [b] Average power conversion efficiency calculated with three individual devices using PCE = P_{out}/P_{in}. (*The average values within the parentheses were obtained from 13 devices)

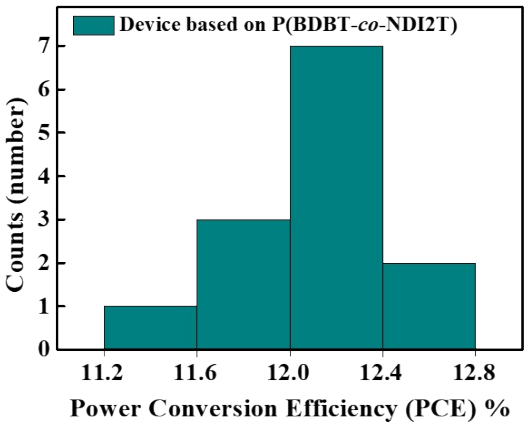

Figure S14. PCE distribution of the optimized IPVs (500 lux). The histogram shows the performance distribution of the 13 devices with the highest efficiency measured in this study. *The active layer was annealed at 120 °C for 10 min.

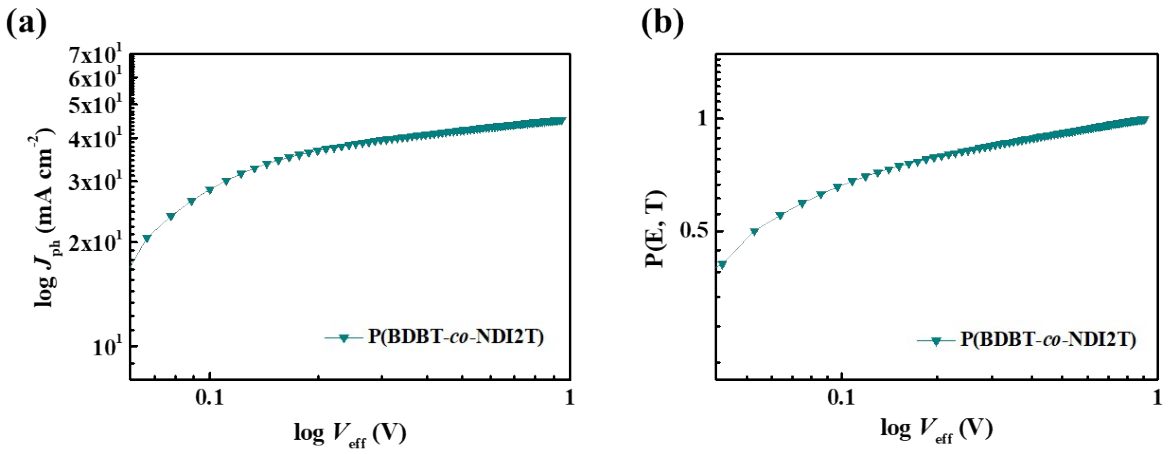

Figure S15. (a) Photocurrent density versus effective voltage characteristics and (b) exciton dissociation probability (plots of J_{ph}/J_{sat} versus effective voltage (V_{eff})) of the IPVs (500 lux) with a photoactive layer of P(BDBT-*co*-NDI2T). *The active layer was annealed at 120 °C for 10 min.

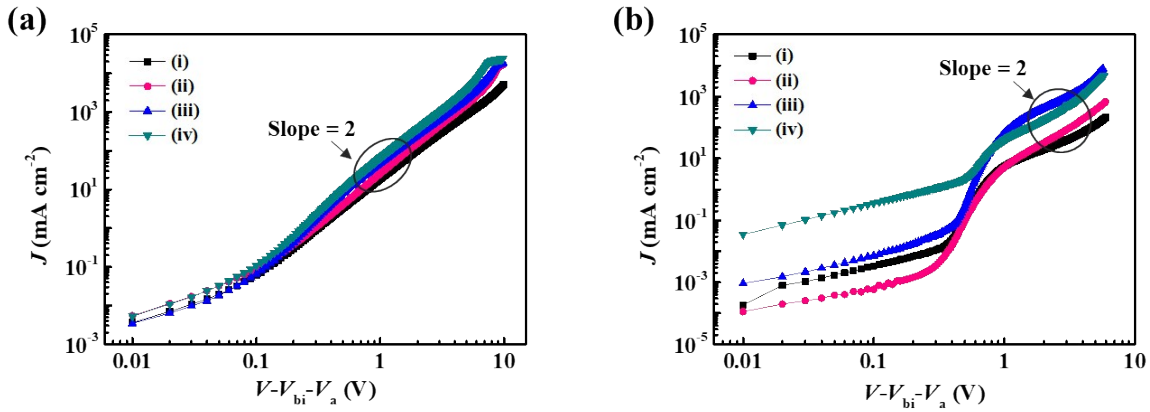

Figure S16. *J–V* characteristics of the polymer films under dark conditions for (a) hole-only devices and (b) electron-only devices. (i) As-cast blend film, (ii) annealed blend film, (iii) as-cast P(BDBT-*co*-NDI2T) film, (iv) annealed P(BDBT-*co*-NDI2T) film.

Table S6. Hole and electron mobilities of the SCLC devices.

Active layer	Treatment	μ_e [cm^2/V·s]	μ_h [cm^2/V·s]	μ_h/μ_e
P(BDBT):P(NDI2T)	As-cast	1.81 x 10^{-6}	1.02 x 10^{-6}	0.56
	120 ℃, 10 min	2.40 x 10^{-6}	1.49 x 10^{-6}	0.62
P(BDBT-*co*-NDI2T)	As-cast	1.59 x 10^{-6}	2.42 x 10^{-6}	1.52
	120 ℃, 10 min	4.87 x 10^{-6}	5.33 x 10^{-6}	1.09

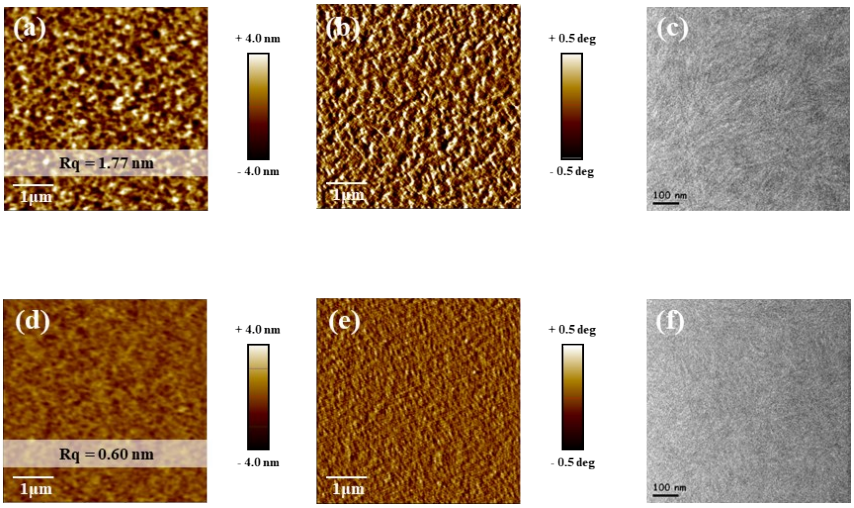

Figure S17. (a, d) AFM height images (b, e) phase images (5μm x 5μm), (c, f) TEM images of the thin films. (a, b, c) as-cast P(BDBT):P(NDI2T) blend (2:1) films, and (d, e, f) as-cast P(BDBT-*co*-NDI2T) films.

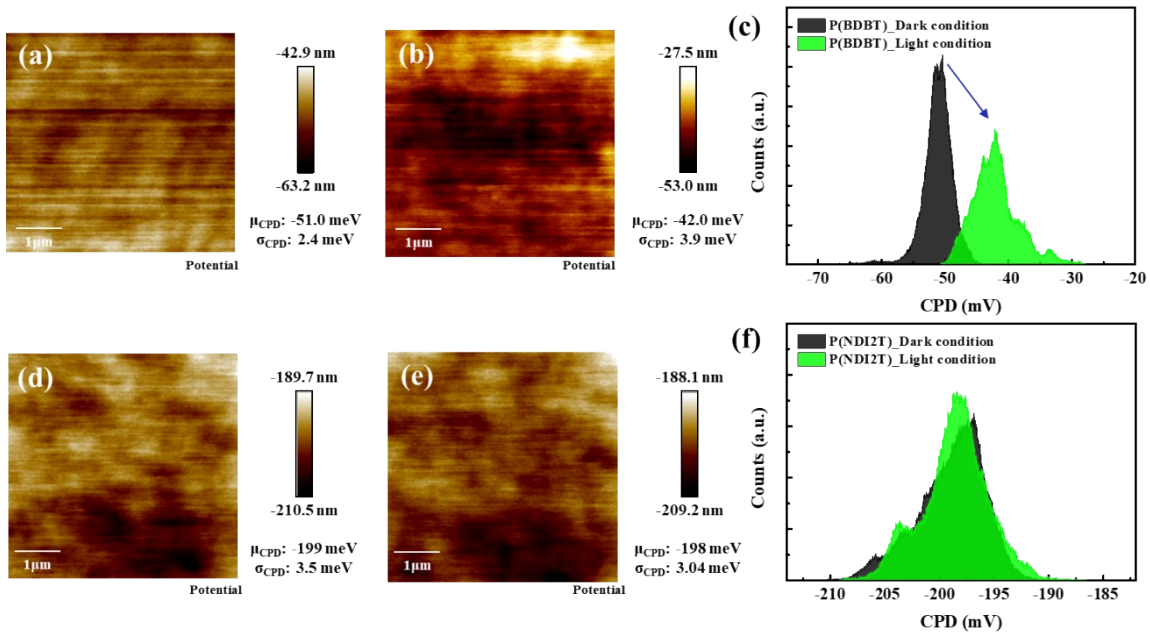

Figure S18. (a, b, d, e) KPFM images with a layer of the annealed P(BDBT) film and annealed P(NDI2T) film (a, d) in the dark and (b, e) under light irradiation (λ=532nm, Applied bias = 2000 mV). (c, f) Histogram of the CPD values in the dark (black) and under light irradiation (λ=532 nm). *The active layer was annealed at 120 °C for 10 min.

Table S7. Summary of KPFM measurements.

	$\mu_{CPD} \pm \sigma_{CPD}$ [meV]		$\Delta\mu_{CPD}$ [b]
	Dark[a]	Light (λ=532 nm) [a]	
P(BDBT)	-51.0±2.4	-42.0±3.9	+9.0
P(NDI2T)	-199.0±3.5	-198.0±3.0	+1.0

[a] Histogram exhibited multimodal distribution. The largest value is displayed here. [b] Difference in μ_{CPD} before and after light irradiation.

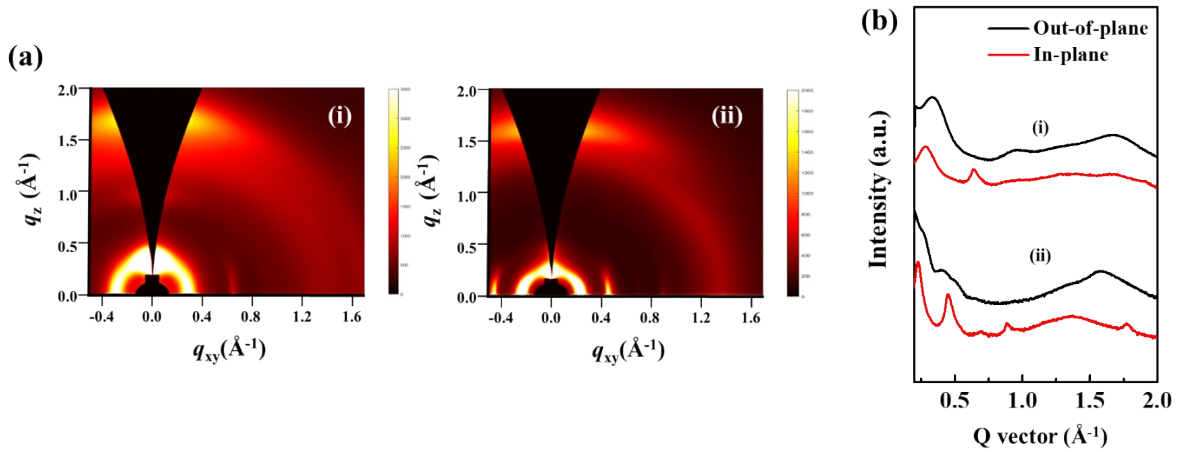

Figure S19. Grazing incidence wide-angle X-ray diffraction data : (a) 2D diffraction pattern and (b) out-of-plane (black lines) and in-plane (red lines) profiles; (i) as-cast P(BDBT) and (ii) as-cast P(NDI2T) film.

Polymer	Temp. [°C]	Plane	Direction	q [Å^{-1}]	d-spacing [Å]	FWHM [Å]
P(BDBT)	As-cast	Out	(010)	1.67	3.70	0.107
		In	(100)	0.28	22.18	0.043
		In	(200)	0.63	9.84	0.024
P(NDI2T)	As-cast	Out	(010)	1.57	3.94	0.110
		In	(100)	0.22	27.66	0.016
		In	(200)	0.44	13.99	0.019

Table S8. Structural parameters of the P(BDBT) and P(NDI2T) films obtained from the GIWAXD measurements.

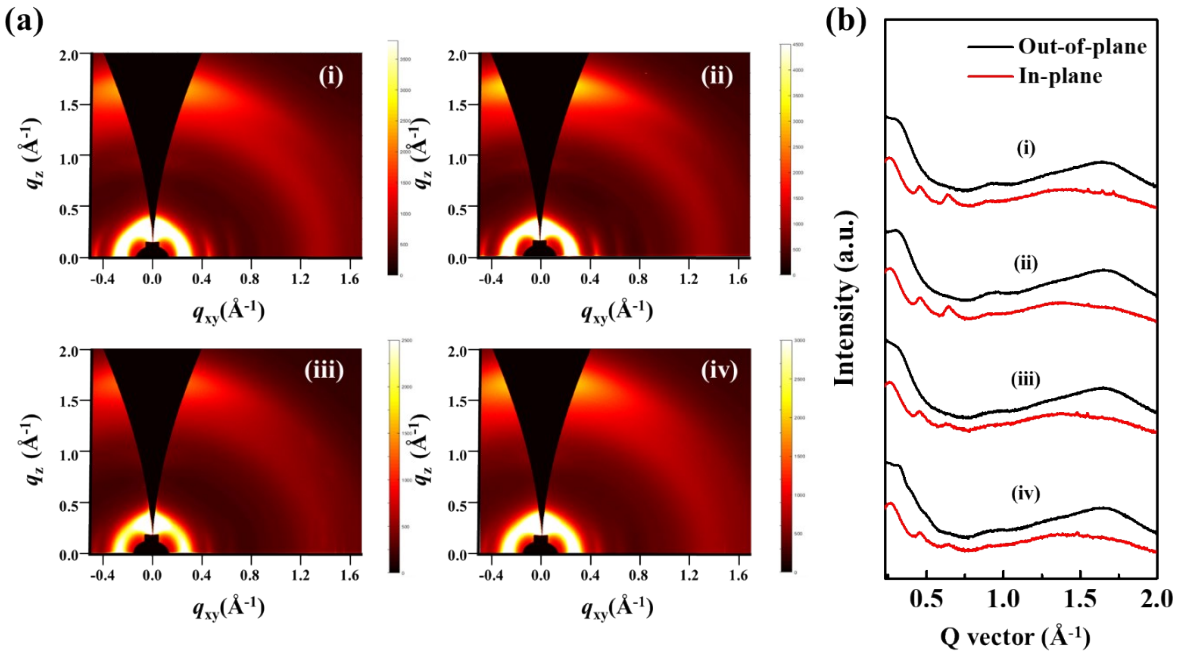

Figure S20. Grazing incidence wide-angle X-ray diffraction data: (a) 2D diffraction pattern and (b) out-of-plane (black lines) and in-plane (red lines) profiles; (i) as-cast blend film, (ii) annealed blend film, (iii) as-cast P(BDBT-*co*-NDI2T) film, and (iv) annealed P(BDBT-*co*-NDI2T) film. *The active layer was annealed at 120 °C for 10 min.

Table S9. Structural parameters of P(BDBT):P(NDI2T) blend and P(BDBT-*co*-NDI2T) films obtained from the GIWAXD measurements.

Polymer	Temp. [°C]	Plane	Direction	q [Å^{-1}]	d-spacing [Å]	FWHM [Å]
P(BDBT):P(NDI2T)	As-cast	Out	(010)	1.64	3.76	0.125
		In	(100)	0.25	24.40	0.034
		In	(200)[a]	0.45	13.91	0.025
		In	(200)[b]	0.63	9.88	0.020
	120 °C	Out	(010)	1.64	3.76	0.121
		In	(100)	0.26	23.78	0.029
		In	(200)[a]	0.45	13.71	0.024
		In	(200)[b]	0.64	9.74	0.026
Polymer	Temp. [°C]	Plane	Direction	q [Å^{-1}]	d-spacing [Å]	FWHM [Å]
P(BDBT-*co*-NDI2T)	As-cast	Out	(010)	1.65	3.74	0.144
		In	(100)	0.25	24.40	0.029
		In	(200)[a]	0.45	13.78	0.021
		In	(200)[b]	0.62	10.05	0.025
	120 °C	Out	(010)	1.64	3.78	0.135
		In	(100)	0.26	23.58	0.028
		In	(200)[a]	0.45	13.78	0.022
		In	(200)[b]	0.63	9.81	0.030

[a] (200) peaks originated from the NDI2T part and [b] from the BDBT part.

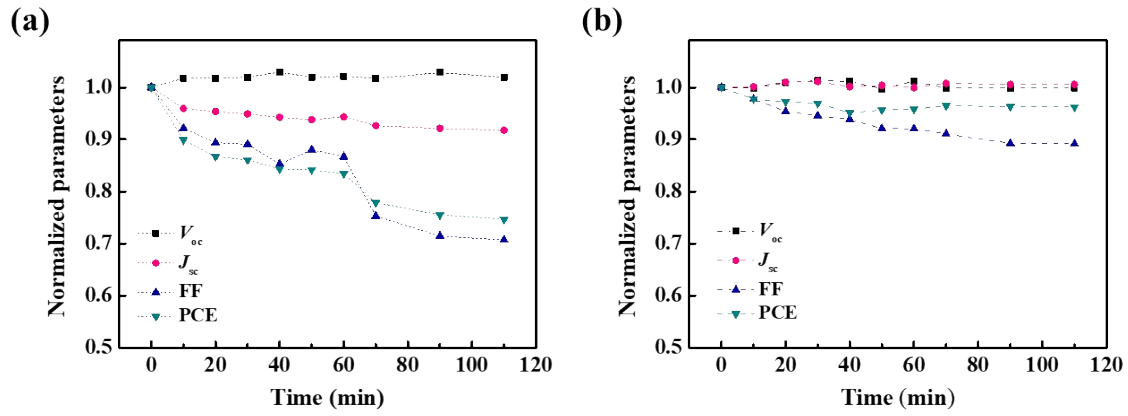

Figure S21. (a) Operational stability of IPVs under LED lamp (500 lux). Active layer: (a) as-cast P(BDBT):P(NDI2T) blend (2:1) films and (b) as-cast P(BDBT-*co*-NDI2T) films.

Notes and references

S1. M. Lenes, M. Morana, C. J. Brabec and P. W. M. Blom, *Adv. Funct. Mater.*, 2009, **19**, 1106-1111.

S2. L. Lu, W. Chen, T. Xu and L. Yu, *Nat. Commun.*, 2015, **6**, 7327.

S3. G. G. Malliaras, J. R. Salem, P. J. Brock and C. Scott, *Phys. Rev. B,* 1998, **58**, 13411.

S4. S. M. Menke, N. A. Ran, G. C. Bazan and R. H. Friend, *Joule*, 2018, **2**, 25-35.

S5. Y. Wang, D. Qian, Y. Cui, H. Zhang, J. Hou, K. Vandewal, T. Kirchartz and F. Gao, *Adv. Energy Mater.*, 2018, **8**, 1801352.

S6. L. J. A. Koster, V. D. Mihailetchi, H. Xie and P. W. M. Blom, *Appl. Phys. Lett.*, 2005, **87**, 203502.

S7. M.-H. Jao, H.-C. Liao and W.-F. Su, *J. Mater. Chem. A*, 2016, **4**, 5784-5801.